

Sections from the Report (2002):

**EUROPEAN COMMISSION (EC) DIRECTORATE-GENERAL ENV.3
PROJECT NO ENV.C.2/SER/2000/ 0064 ‘DRAWING UP AND EVALUATING
REMEDIAION STRATEGIES FOR THE CHERNOBYL COOLING POND’,**

**TASK 2: BACKGROUND OF SCENARIOS AND MODELLING OF THE
PATHWAYS**

**SUBTASK: 2.3. ASSESSMENT OF DOSES TO POTENTIAL
EXPOSURE GROUPS FROM COLLAPSE OF THE DAM**

Sergey Kivva and Mark Zheleznyak
Ukrainian Center of Environmental and Water Projects
Prospect Glushkova, 42, Kiev, 03187, Ukraine
mark@immisp.kiev.ua

CONTENTS

INTRODUCTION.....	2
1. PREPARATION OF THE DIGITAL GEOSPATIAL DATA FOR THE SIMULATION OF THE DAM BREAK PROBLEM.....	3
2. TWO DIMENSIONAL MODELLING OF THE WATER FLOW AND RADIONUCLIDE TRANSPORT IN VICINITY OF THE COOLING POND FOR DIFFERENT SCENARIOS OF THE DAM BREAK.....	9
2.1. MATHEMATICAL MODEL	9
2. 3 SIMULATED RESULTS	9
REFERENCES TO CHAPTER 2	21
ANNEX 1: 2-D MODEL USED TO SIMULATE WATER FLOW, SEDIMENT AND RADIONUCLIDE TRANSPORT IN THE VICINITY OF THE DAM BREAK.....	22
2.1. MATHEMATICAL MODEL	22
<i>Overland Flow.....</i>	22
<i>Erosion/Deposition and Sediment transport.....</i>	22
<i>Radionuclide Transport by Overland Flow.....</i>	24
<i>Contamination of Upper Soil Layer.</i>	24
NUMERICAL METHODS	24
<i>Overland Flow.....</i>	25
<i>Advective-Dispersive Transport Equation.....</i>	27
<i>Approximation of the Boundary Condition.....</i>	28
<i>Numerical solution of the descretized equations.....</i>	28
REFERENCES TO ANNEX 1.....	29

Introduction

The approved working plan of this Subtask includes

1. Preparation of the digital geospatial data for the simulation of the dam break problem
2. Two dimensional modelling of the water flow and radionuclide transport in vicinity of the Cooling Pond for different scenarios of the dam break
3. One –dimensional modelling of radionuclide transport through the Dnieper reservoirs cascade on the basis of the fluxes from Pripyat River calculated as the output from the dam break problem.
4. Assessment of doses for population assuming Dnieper water on the basis of the scenarios of radionuclide concentration in Dnieper after the collapse of the Cooling pond's dam

The results of the data processing and simulations, provided in accordance with this plan, are presented in four Chapters of this report. The descriptions of the models are presented in 4 annexes.

1. Preparation of the digital geospatial data for the simulation of the dam break problem

To prepare the digitised geospatial input data for the modelling of the consequences of the potential dam break it was provided specialised study «Creation of the Unified Digital Model of ChNPP Cooling Pond and Territories of the Near Zone of Spreading of Potential Wave Break – from Yanov creek to Chernobyl». The aim of the above work was creating on the GIS platform of information base for the modelling systems allowing automating the process of the data preparation (topographical marks of surface, density of territory and bottom contamination with ^{90}Sr and ^{137}Cs) in order to simulate and compare the data of various sources on the spatial basis.

In the process of implementation of the first stage of works the information base integrating the listed below on the unified spatial basis was created on GIS platform ArcInfo:

1. Digital map of the Exclusion Zone territory, scale 1:25 000, including data of relief structure and hydrography;
2. Digital map of the territory adjacent to the Cooling Pond, scale 1:10 000, including data of relief structure and hydrography;
3. Digital map of Cooling Pond bottom relief isolines;
4. Digital maps of isolines of density of Exclusion Zone soil contamination with ^{90}Sr and ^{137}Cs , scale 1:200 000;
5. Digital maps of isolines of density of Exclusion Zone soil contamination with ^{90}Sr and ^{137}Cs , created upon the data of bottom sediments' sampling.

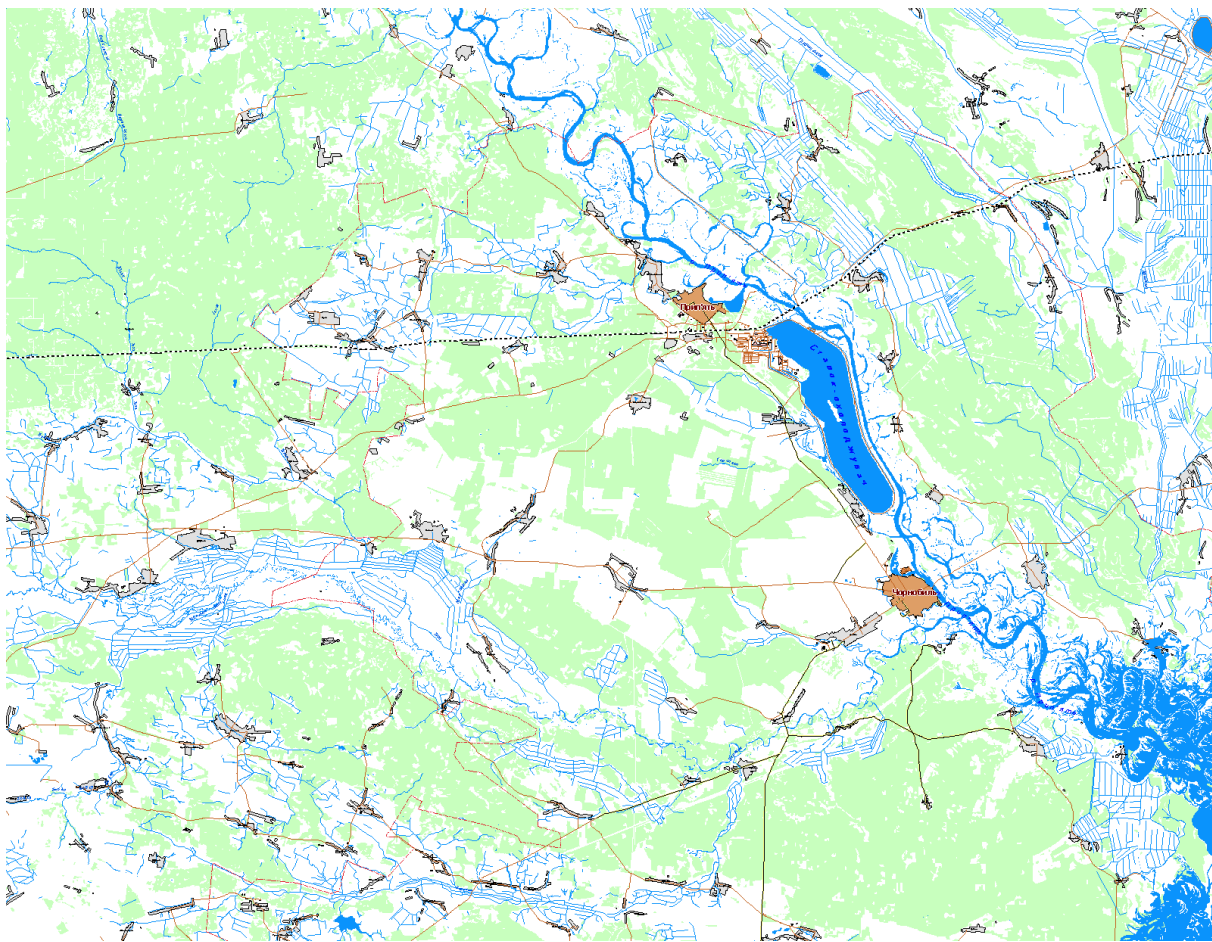


Fig. 1. 1. Digitized map of the Exclusion Zone, scale 1:25 000

The task for the following stage was transformation of the data of the existing digital maps of relief and radionuclide contamination into the continuous surfaces with further transfer into computational model grid (GRID).

In order to create the digital model of relief (DEM) of the considered territories the data of maps with scales 1:25000 and 1:10000 were used (isolines, relief marks, hydronetwork). Relief of the Cooling Pond bottom was created based upon the data of depth measurements presented in relevant section of this report in the format of “Surfer 6” software. The development was performed in the Arc/Info GIS environment with the use of function Topogrid.

The surface models of contamination of studied territory with strontium and caesium were created by way of interpolation of data of digital maps of contamination density of the Exclusion Zone territory (scale 1:200 000), presented by the Institute of Agriculture Radioecology (the group lead by Dr. V. Kashparov). The method of creation of surface data foresees the interpolation of isolines of contamination by method of triangulation of irregular network (TIN) with further transformation into Grid by means of Arc/Info. The surface of density of contamination of the Cooling Pond was obtained by the same way on the basis of sampling data of the bottom sediments, transferred by group of UHMI (V. Kanivets, V. Lutkovsky) in format Surfer 6.

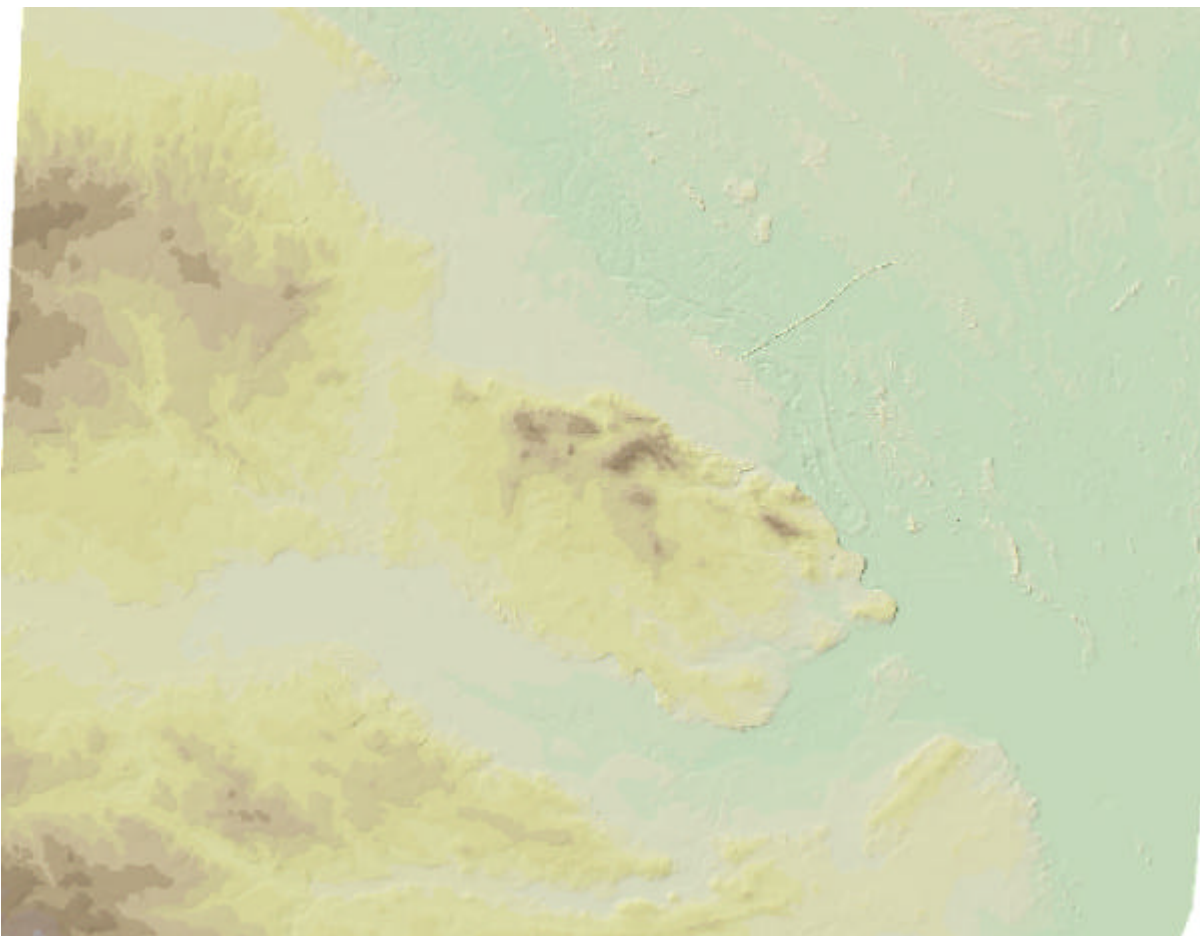


Fig.1. 2. Digital Elevation Model (DEM) of Exclusion Zone, created based upon the data of scale 1:25 000

In the result of the work under this stage the following data were created:

1. The model of surface relief (DEM) of the Exclusion Zone territory, created based upon the data of a map of scale 1 : 25 000 in format GRID;
2. The model of surface relief (DEM) of the Exclusion Zone territory, adjacent to the Cooling Pond, created based upon the data of a map of scale 1 : 10 000 in format GRID;
3. The model of surface relief (DEM) of the Cooling Pond bottom, created based upon the data of bottom relief measurements in format GRID;
4. The model of the Exclusion Zone territory contamination with ^{137}Cs , created based upon the data of a map of isolines of contamination density, scale 1 : 200 000 in format GRID;
5. The model of the Exclusion Zone territory contamination with ^{90}Sr , created based upon the data of a map of isolines of contamination density, scale 1 : 200 000 in format GRID;
6. The model of surface contamination of the bottom of Cooling Pond with ^{137}Cs , created on the basis of sampling data of the bottom sediments in format GRID;
7. The model of surface contamination of the bottom of Cooling Pond with ^{90}Sr , created on the basis of sampling data of the bottom sediments in format GRID;

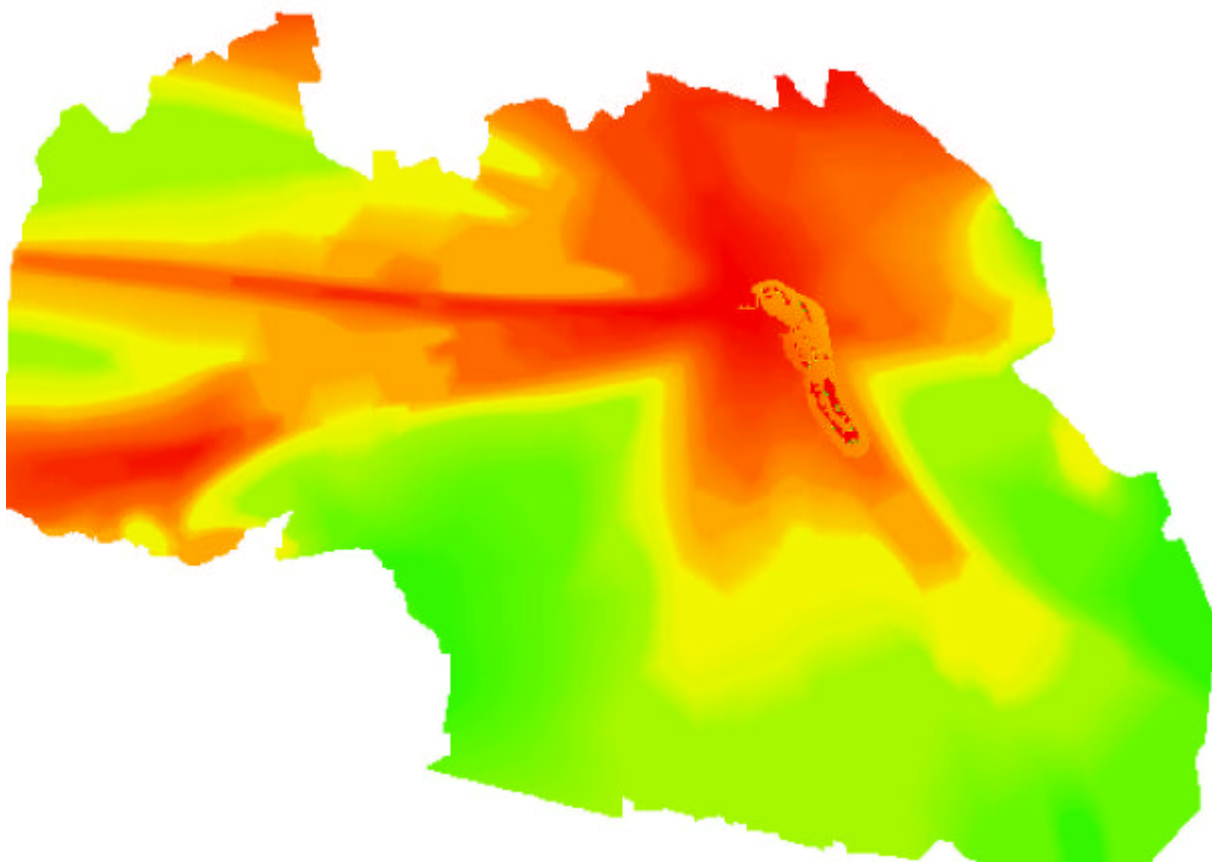


Fig. 1. 3. The model of surface of contamination of the Exclusion Zone territory with ^{137}Cs in format GRID

On the final stage of these investigations the following main tasks were solved:

- ? Integration of surfaces of the same kind into the combined resultant surface reflecting the picture of distribution of parameter with the necessary detailing for each area.
- ? Re-formatting of the obtained surfaces from format GRID ArcInfo into buffer format ASCII for transfer into computation grid of model.



Fig. 1.4. The result of integration of the model of the Exclusion Zone surface relief created upon the data of map with scale 1:10 000 with the model of the Cooling Pond bottom relief

In the process of works under this stage the following information layers were obtained and transferred into simulating system in format ASCII:

1. Combined model of surface relief (DEM) of the Exclusion Zone territory, created based upon the data of maps with scales 1 : 25 000, 1:10 000 and bottom relief measurements;
2. Combined model of the Exclusion Zone territory density of contamination with ^{137}Cs , created based upon the data of map of isolines of contamination density with scale 1 : 200 000 and sampling of the Cooling Pond bottom sediments;
3. Combined model of the Exclusion Zone territory density of contamination with ^{90}Sr , created based upon the data of map of isolines of contamination density with scale 1 : 200 000 and sampling of the Cooling Pond bottom sediments.



Fig. 1.5. Result of integration of surface models contaminated with ^{90}Sr (territory of Exclusion Zone (GRID) and bottom of Cooling Pond)

2. Two dimensional modelling of the water flow and radionuclide transport in vicinity of the Cooling Pond for different scenarios of the dam break

2.1. Mathematical model

Two dimensional lateral longitudinal radionuclide transport model COASTOX have been used to simulate overland flow, suspended sediment transport and radionuclide transport both in the cooling pond and on the neighbouring floodplaine after the dam break. The model was tested within different studies of the radionuclide transport in the Chernobyl zone (Zheleznyak at al., 1992, 1997, Zheleznyak, 1997) and it is included into the Hydrological Dispersion Modeule of the EU decision support system RODOS (Zheleznyak, Raskob and Heling, 2002). The model has been recently applied to simulate radionuclide wash –of from small watersheds (Kivva, Zheleznyak, 2001; van der Perk et al., 2000). Within the projecvt the numerical methods was refined for the model implementation for dam break problem.

The model consists of the modules describing overland flow; sediment transport; erosion/deposition processes; radionuclide transport in solute and on suspended sediments by the overland flow and contamination of upper soil layer. The model and numerical methods are presented in the Annex 1.

2. 3 Simulated Results

The objectives of the simulations were to evaluate discharge of ^{137}Cs and ^{90}Sr in the Pripjat river due to partial dam-break of the Cooling Pond of the Chernobyl NPP. The computational domain was defined by area about 22200 m long, 13000 m wide, near the Chernobyl NPP. It was considered two cases of partial dam-break problem: (1) with breach of 60 m in length, and (2) with breach of 150 m in length. It was assumed that bed elevation of the dam breaches was at 105 m. The dam failure occurs instantaneously at time $t=0$. The initial water level in the Cooling Pond was at 110.6 m. The initial sediment concentration in the Cooling Pond was 0.01 kg m^{-3} , and in the Pripjat river was 0.06 kg m^{-3} . The initial total radionuclide concentration of ^{137}Cs equals to 2.4 pCi/l in the Pripjat river and 70.3 pCi/l in the Cooling Pond. For ^{90}Sr these initial concentration were 8.0 pCi/l and 51.4 pCi/l, respectively. Values of parameters used in numerical simulations for erosion/deposition processes are given in Table 1.

Table 1. Values of parameters used for simulation of erosion/deposition processes.

Sediment particle size, μm	$\tau_d, \text{N m}^{-2}$	$\tau_e, \text{N m}^{-2}$	Sediment density, kg m^{-3}	$M, \text{kg m}^{-2} \text{ s}^{-1}$
10	0.1	2.5	2500	$3 \cdot 10^{-5}$

The hydraulic boundary conditions for the Pripjat river were fixed water discharge of 670 m^3 per s upstream and fixed water level at 103 m downstream.

The computational domain was discretized by a non-uniform rectangle mesh, the nodes of which were spaced at 30 m – 210 m intervals in the length, and from 30 to 150 m in the width. Initial velocity field in the Pripjat river is shown in Fig.1. Values for species properties used in the simulations of radionuclide contamination are presented in Table 2. Results of the simulations are illustrated in Fig.2-15.

Table 2. Values of parameters used in simulations of radionuclide transport.

nuclide	k_d^b (m ³ /kg)	k_d^s (m ³ /kg)	a_b (1/day)	a_s (1/day)
¹³⁷ Cs	10	30	1	0.00274
⁹⁰ Sr	2	3	1	0.00274

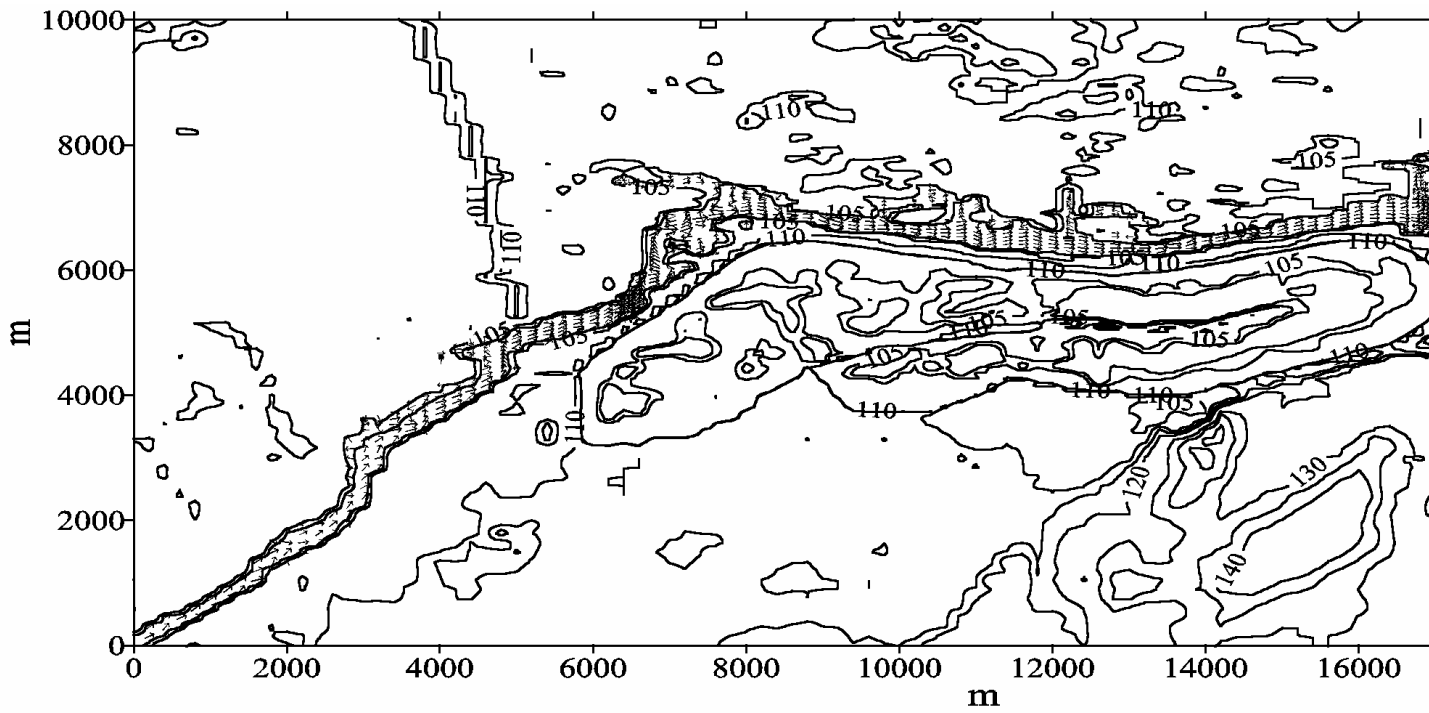


Fig. 2.1. Elevation map and initial velocity field in the Pripjat river near the Chernobyl NPP.

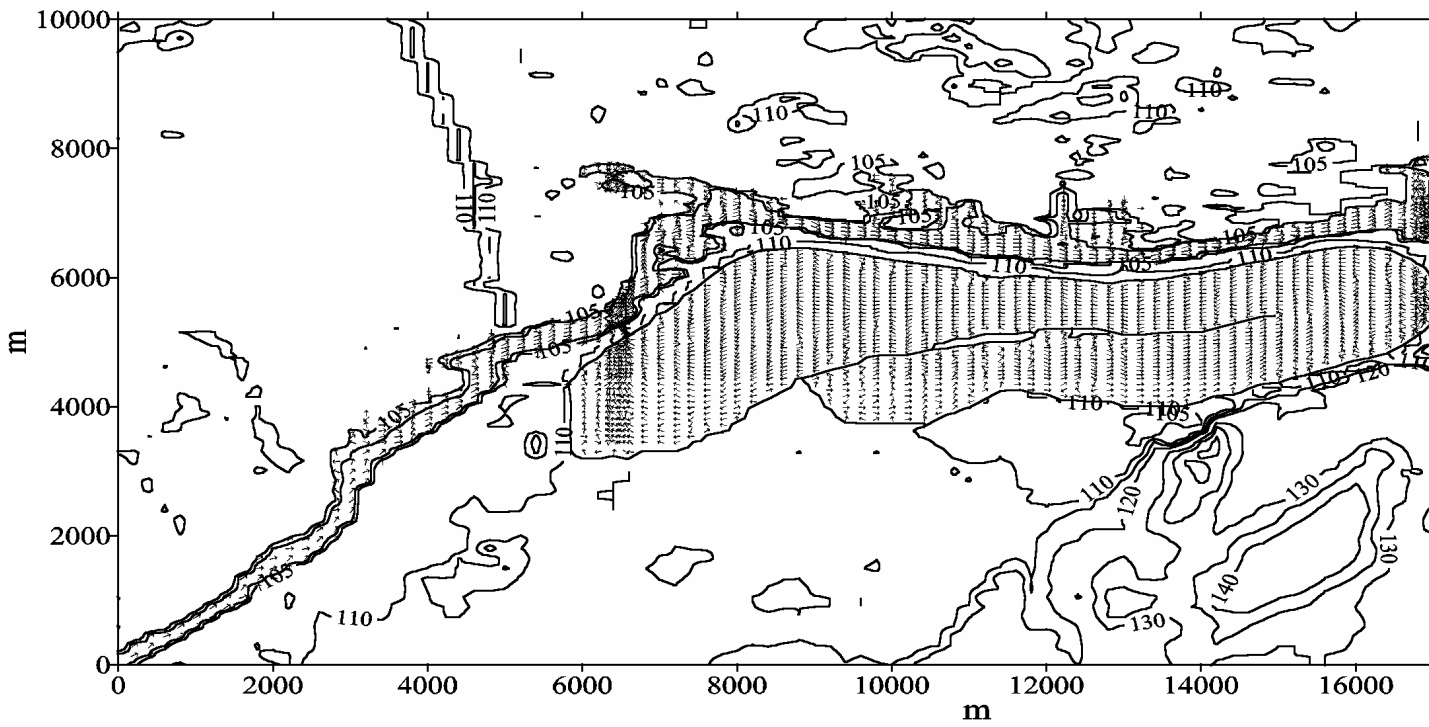


Fig. 2.2. Velocity field of water flow at time $t=500$ min after dam failure with 60m-breach.

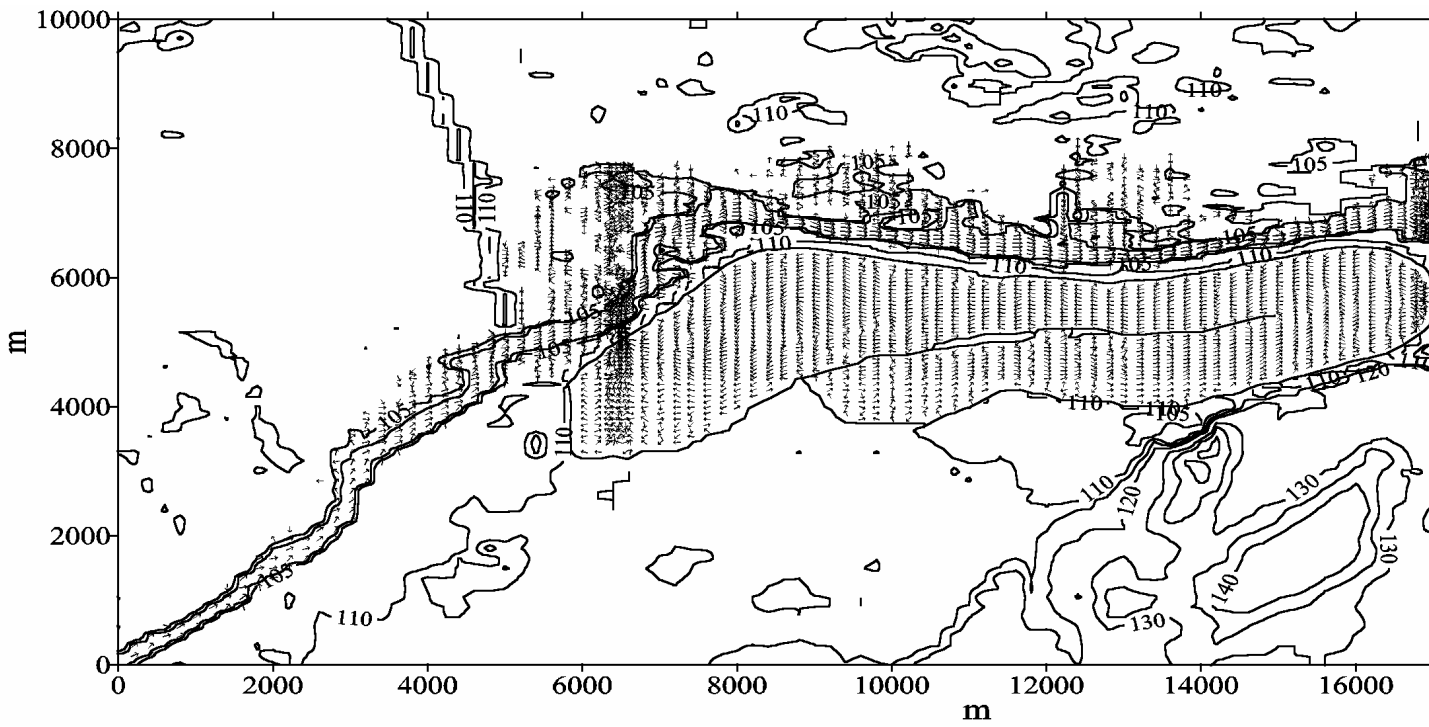


Fig. 2.3. Velocity field of water flow at time $t=500$ min after dam failure with 150m-breach.

The following figures below illustrate dynamics of surrounding territory inundation after dam failure with 150-m breach.

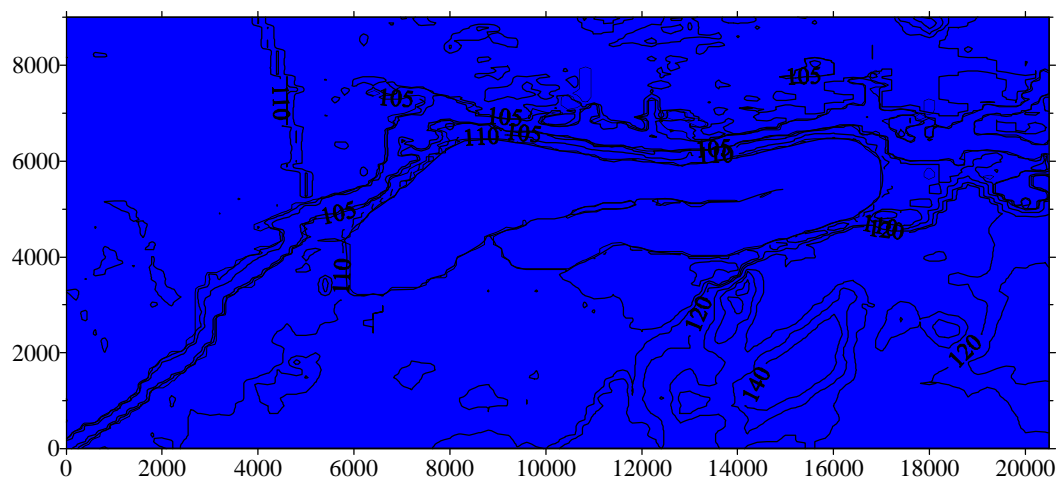


Fig.2.4. Inundated territory after 30 s after dam failure with 150-m breach.

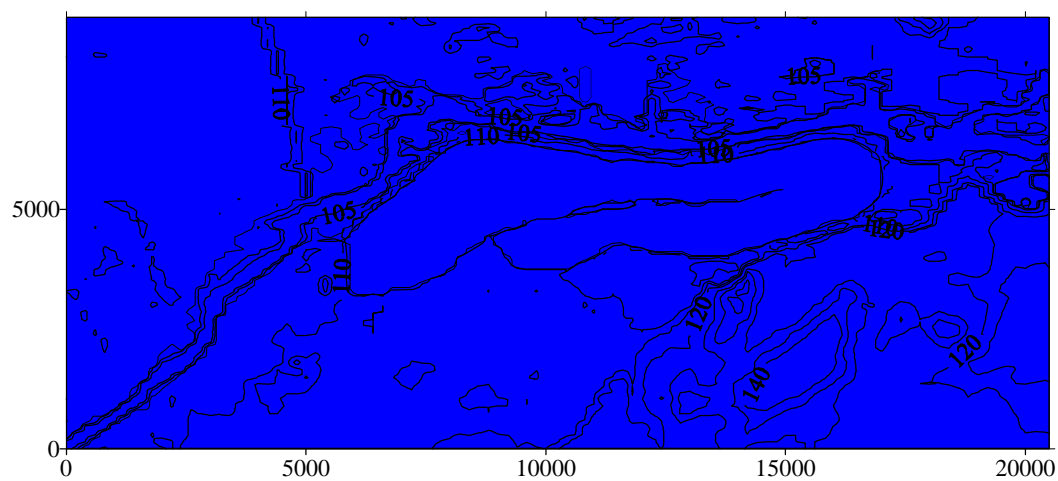


Fig.2.5. . Inundated territory after 200 min after dam failure with 150-m breach.

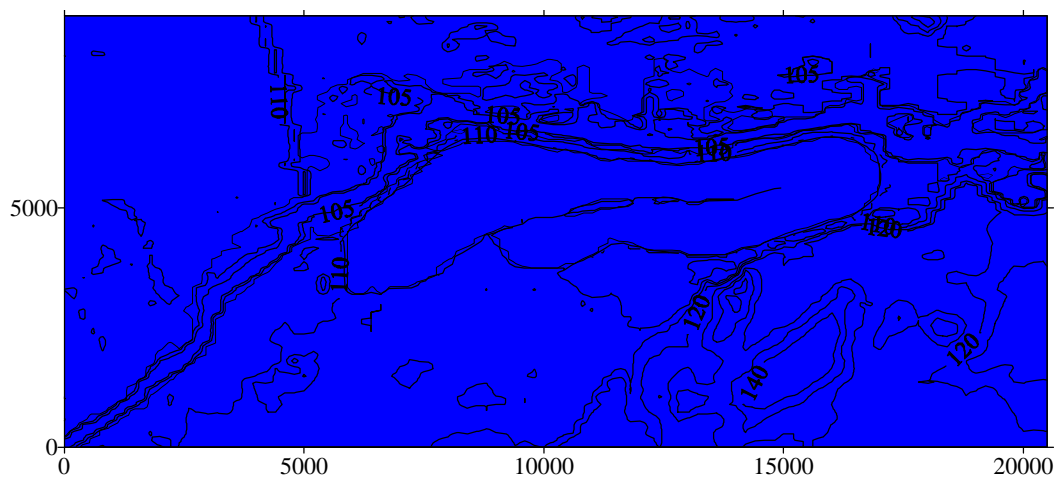


Fig.2.6 Inundated territory after 500 min after dam failure with 150-m breach.

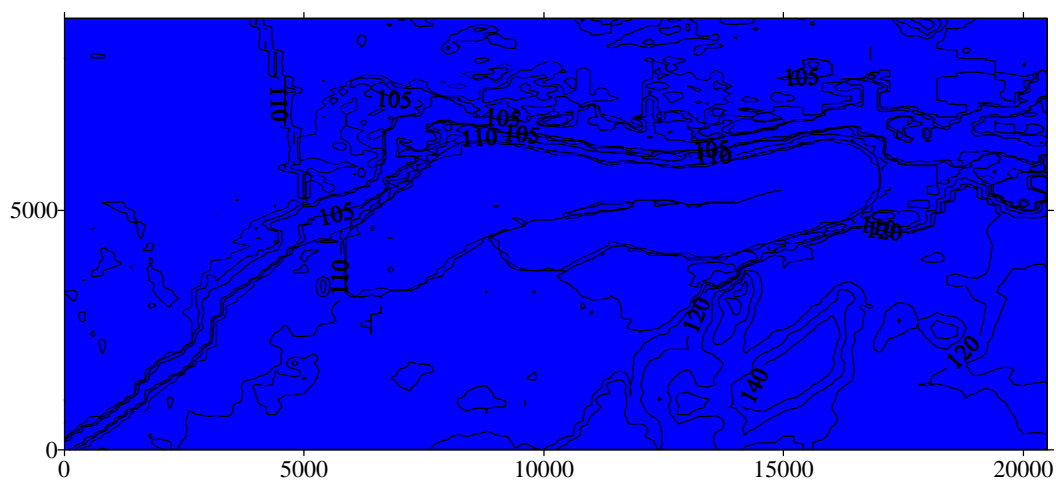


Fig.2.7 . Inundated territory after 800 min after dam failure with 150-m breach.

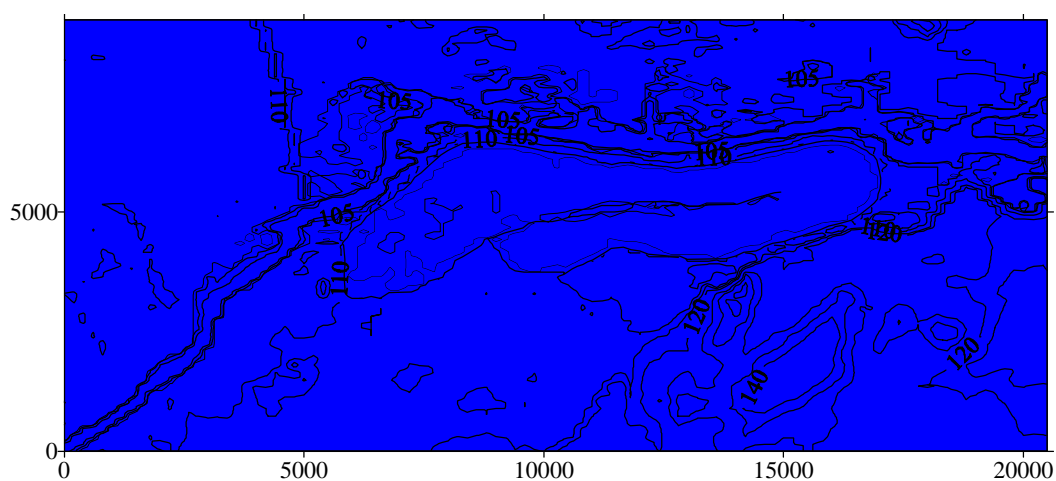


Fig.2.8 . Inundated territory after 30 h after dam failure with 150-m breach.

The figures below present the results in the cross-section of the breach

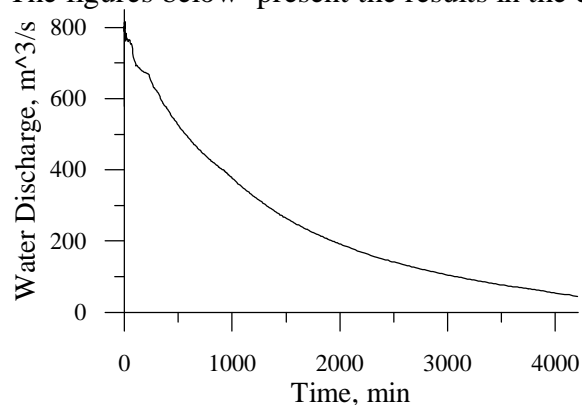


Fig.2.9. Water discharge for dam breaking with 60m-breach.

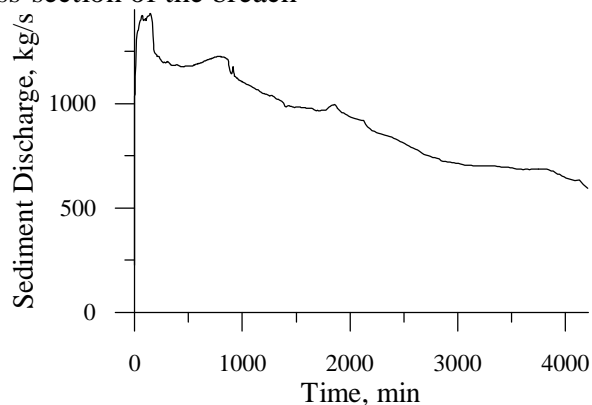


Fig.2.10. Sediment discharge for dam breaking with 60m-breach.

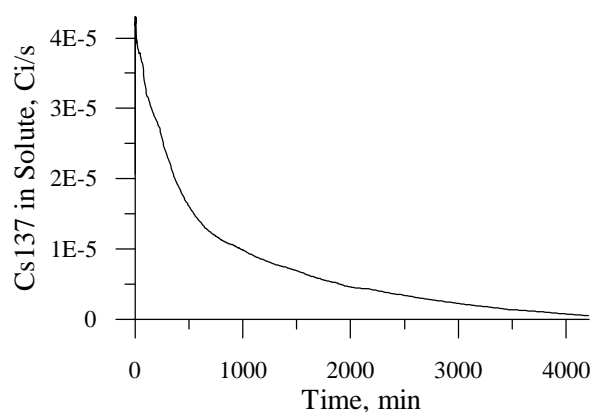


Fig.2.11. Discharge of ^{137}Cs in solute for 60m-breach.

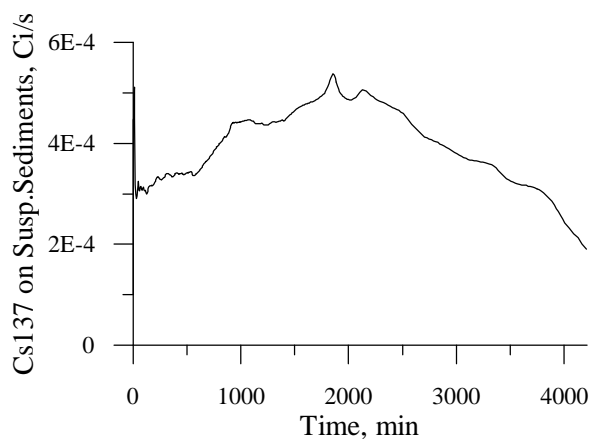


Fig.2.12. Discharge of ^{137}Cs on suspended sediments for 60m-breach.

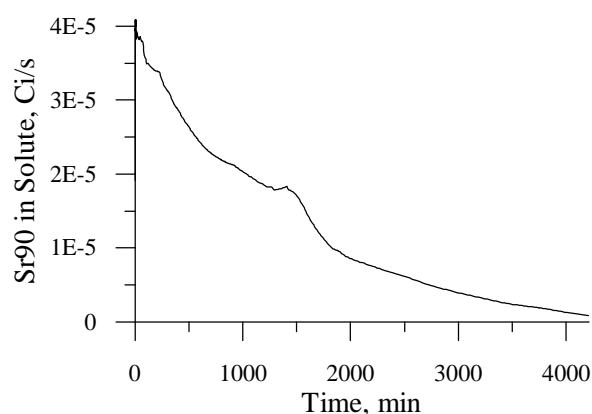


Fig.2.13. Discharge of ^{90}Sr in solute for 60m-breach.

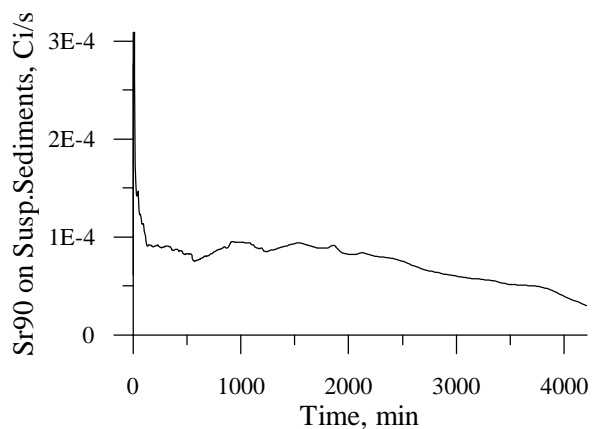


Fig.2.14. Discharge of ^{90}Sr on suspended sediments for 60m-breach.

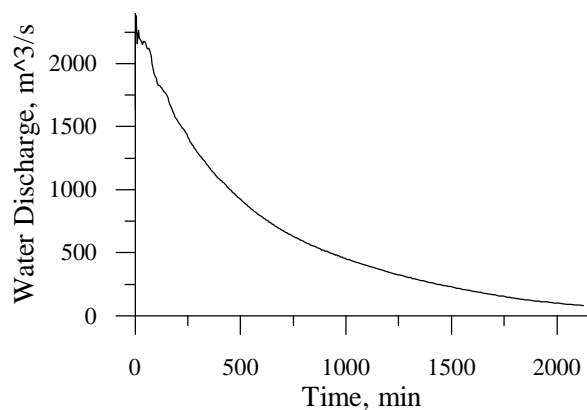


Fig.2.15. Water discharge for dam breaking with 150m-breach.

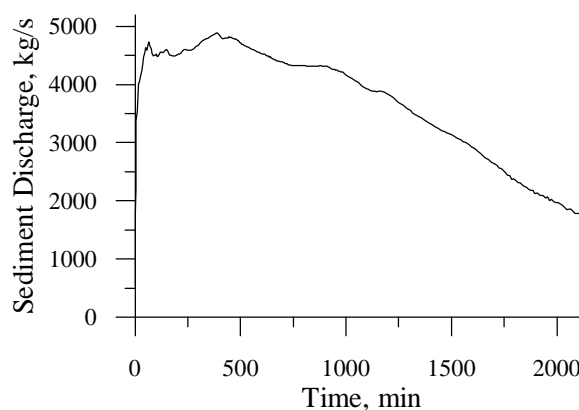


Fig.2.16. Sediment discharge for dam breaking with 150m-breach.

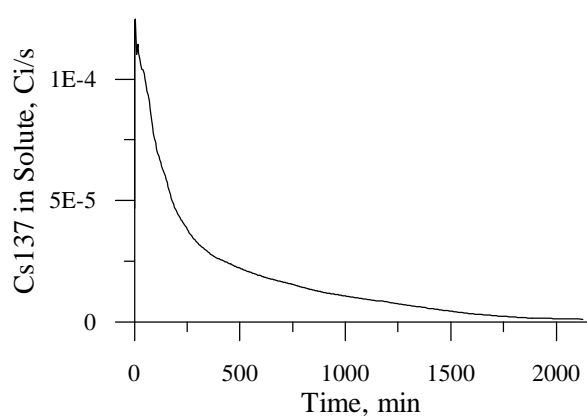


Fig.2.17. Discharge of ^{137}Cs in solute for 150m-breach.

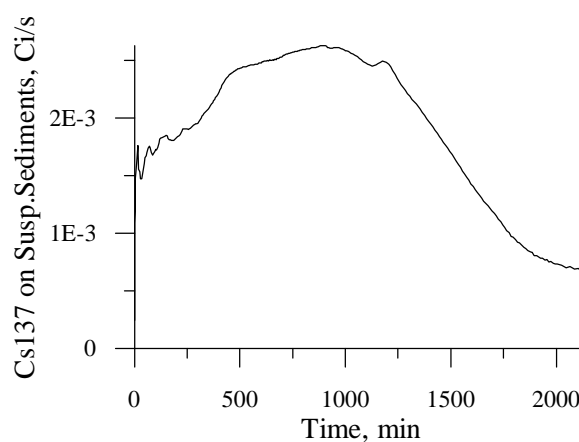


Fig.2.18. Discharge of ^{137}Cs on suspended sediments for 150m-breach.

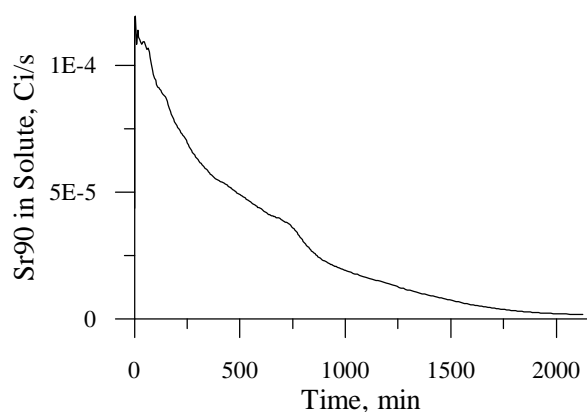


Fig.2.19. Discharge of ^{90}Sr in solute for 150m-breach.

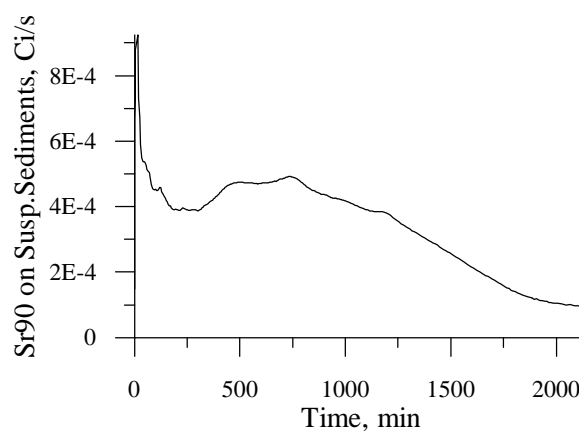


Fig.2.20. Discharge of ^{90}Sr on suspended sediments for 150m-breach.

The figures below present the results for the Pripyat river cross-section at the downstream end of the Cooling Pond (at the city of Chernobyl)

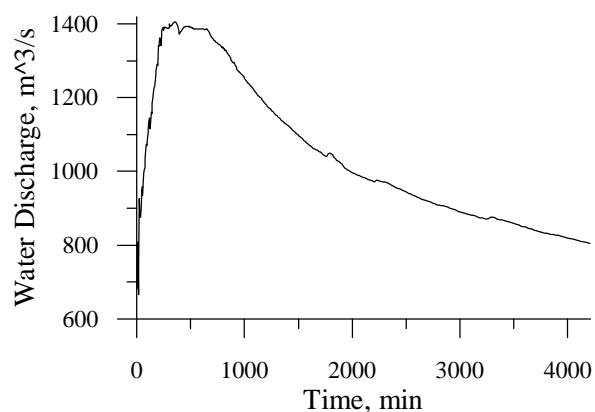


Fig.2.21. Water discharge for dam breaking with 60m-breach.

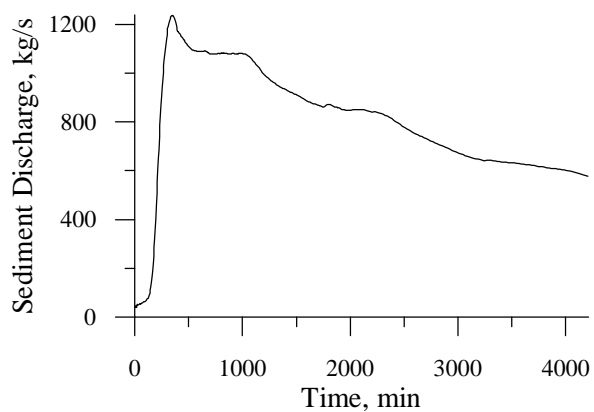


Fig 2..22 Sediment discharge for dam breaking with 60m-breach.

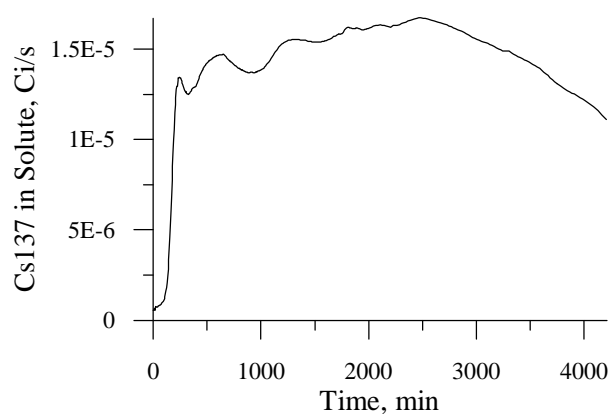


Fig.2.23. Discharge of ^{137}Cs in solute for 60m-breach.

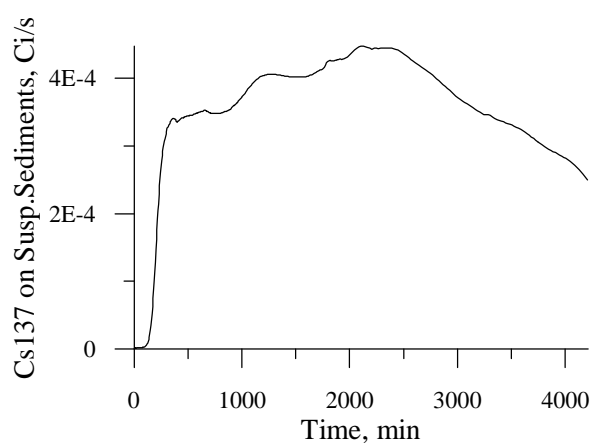


Fig.2.24. Discharge of ^{137}Cs on suspended sediments for 60m-breach.

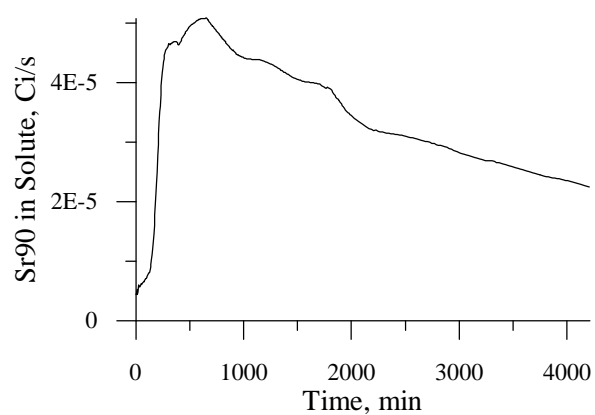


Fig.2.25. Discharge of ^{90}Sr in solute for 60m-breach.

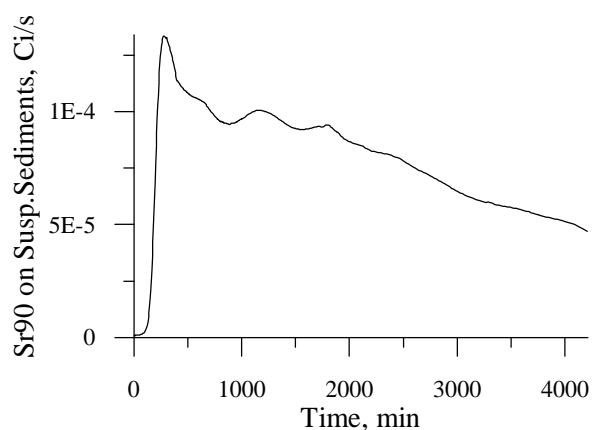


Fig.2.26. Discharge of ^{90}Sr on suspended sediments for 60m-breach.

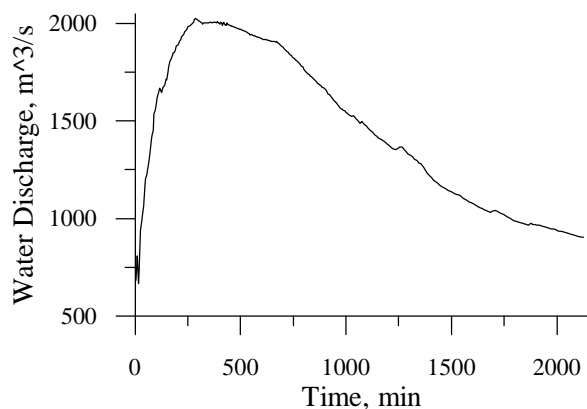


Fig.2.27. Water discharge for dam breaking with 150m-breach.

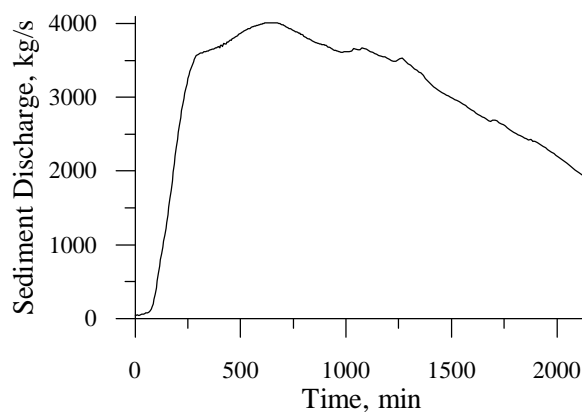


Fig.2.28. Sediment discharge for dam breaking with 150m-breach.

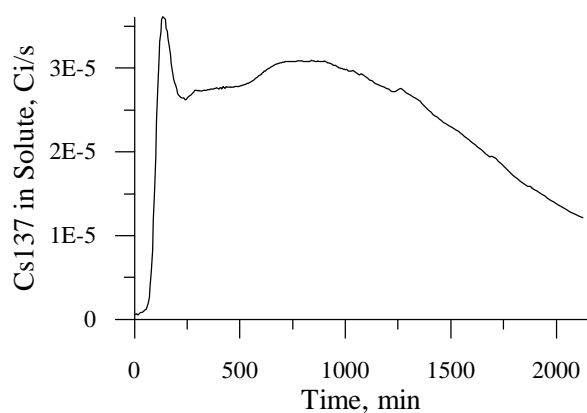


Fig.2.29. Discharge of ^{137}Cs in solute for 150m-breach.

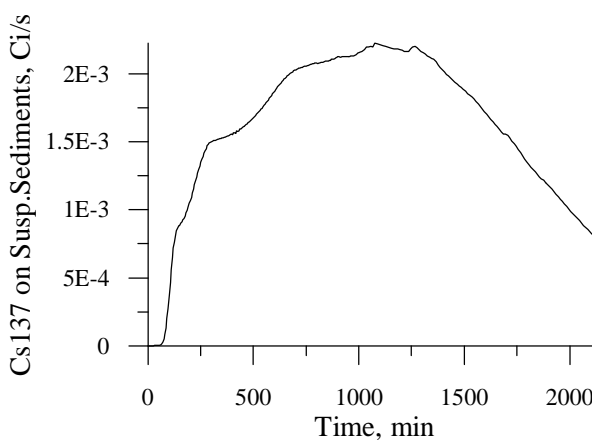


Fig.2.30. Discharge of ^{137}Cs on suspended sediments for 150m-breach.

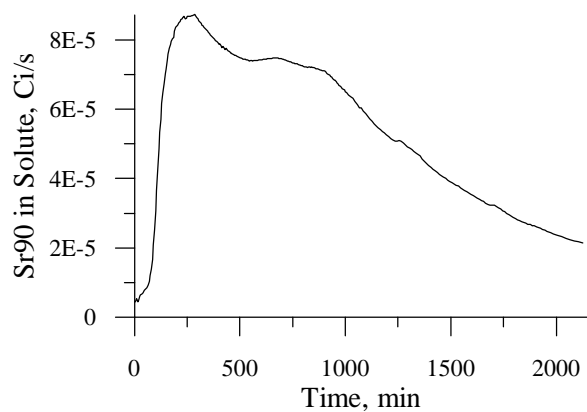


Fig.2.31. Discharge of ^{90}Sr in solute for 150m-breach.

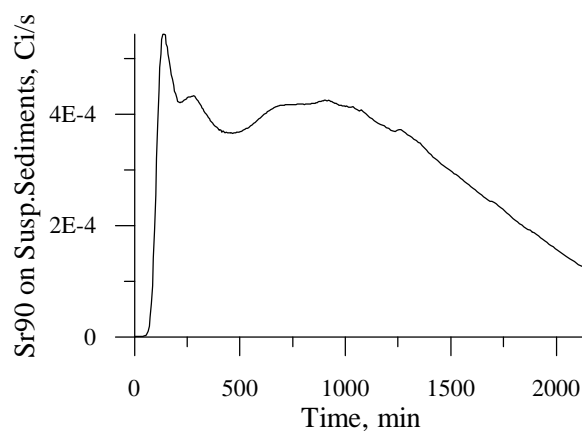


Fig.2.32. Discharge of ^{90}Sr on suspended sediments for 150m-breach.

The simulation results shows that radionuclide discharge in the cross-section of Pripyat river is determined by the radionuclide discharge in the cross-section of dam breach. The radionuclide discharge in soluble form of ^{90}Sr in the Pripyat cross-section increase approximately in 11 and 20 times for dam failure with 60m- and 150m-breach, respectively.

Similarly the discharge of ^{137}Cs in soluble form in cross-section of Pripyat river increase approximately in 29 and 64 times.

The output of the 2-D modeling integrated over cross-section downstream the Cooling Pond has been used as input data to the 1- D model, transporting the radionuclide over whole Dnieper reservoir cascade.

References to Chapter 2

1. Kivva S.L., Zheleznyak M.J. (2001) Numerical modelling of the 2-D open flow with the moving boundaries: simulation of the watershed runoff and tsunami wave runup. *Computational Technologies*, Novosibirsk, , v.6., No2, p. 343-350 (In Russian).
2. Van der Perk M., Jetten V., Karsenberg D., Walling E., Laptev G., Voitsekhovich O., Svetlichnyi A., Slavik O., Linnik V., Korobova E., Kivva S., Zheleznyak M. (2000) Assessment of spatial redistribution of Chernobyl –derived radiocaesium within catchments using GIS-embedded models. – *The Role of Erosion and Sediment Transport in Nutrient and Contaminant Transfer.*, IAHS Publ.No.263, pp.277-284.
3. Zheleznyak M. (1997) Multiple scale analyses of radioactive contamination for rivers and reservoirs after the Chernobyl accident. - Multiple Scale Analyses and Coupled Physical Systems. Proc. Saint-Venant Symposium, August 28-29, 1997, Presses de l'école nationale des ponts et chaussees, Paris, 1997, p.p. 45-52.
4. Zheleznyak M. et al. (1992) Mathematical modeling of radionuclide dispersion in the Pripyat-Dnieper aquatic system after the Chernobyl accident. -*The Science of the Total Environment*, v.112, p.89-114.
5. Zheleznyak M., Heling R., Raskob W. (2002) Hydrological Dispersion Module of the Decision Support System RODOS- Proc. Conf. ECORAD-2001, Aix-de Provance, France, 3-6 September, 2001 (In Press)
6. Zheleznyak M., Shepeleva T., Sizonenko V., Mezhueva I. (1997) Simulation of countermeasures to diminish radionuclide fluxes from Chernobyl zone via aquatic pathways - *Radiation Protection Dosimetry*, 1997, v.73, No.1-4, pp.181-186

ANNEX 1: 2-D model used to simulate water flow, sediment and radionuclide transport in the vicinity of the dam break

2.1. Mathematical model

Two dimensional lateral longitudinal radionuclide transport model COASTOX have been used to simulate overland flow, suspended sediment transport and radionuclide transport both in the cooling pond and on the neighbouring floodplains after the dam break. The model was tested within different studies of the radionuclide transport in the Chernobyl zone (Zheleznyak et al., 1992, 1997, Zheleznyak, 1997) and it is included into the Hydrological Dispersion Module of the EU decision support system RODOS (Zheleznyak, Raskob and Heling, 2002). The model has been recently applied to simulate radionuclide wash-off from small watersheds (Kivva, Zheleznyak, 2001; van der Perk et al., 2000). Within the project the numerical methods were refined for the model implementation for dam break problem.

The model consists of the modules describing overland flow; sediment transport; erosion/deposition processes; radionuclide transport in solute and on suspended sediments by the overland flow and contamination of upper soil layer. The model is presented in details in the Annex 1.

Overland Flow

Two-dimensional overland flow equations are obtained by vertically averaging the three-dimensional equations over flow depth and using the above kinematic boundary conditions. These equations consist of a continuity equation and two momentum equations. These equations can be expressed as follows

$$\frac{\partial h}{\partial t} + \frac{\partial}{\partial x_i} (u_i h) = 0 \quad (1)$$

$$\frac{\partial}{\partial t} (u_i h) + \frac{\partial}{\partial x_j} (u_j u_i h) + gh \frac{\partial z}{\partial x_i} - g \frac{n^2}{h^{4/3}} u_i \sqrt{u_1^2 + u_2^2} = 0 \quad (2)$$

where t is the time variable (s); x_i is the spatial Cartesian coordinates (m); h is the flow depth (m); u_i is the flow velocity in the x_i -direction (m s^{-1}); $z(x,y,t)$ is the free surface elevation (m); $z_b(x,y,t)$ is the bed surface elevation (m); g is the acceleration of the gravity (m s^{-2}); n is the Manning roughness coefficient ($\text{s m}^{-1/3}$).

Erosion/Deposition and Sediment transport.

Change of the bed surface elevation is described by

$$\frac{\partial z_b}{\partial t} = q_s - q_b$$

where ϕ is the porosity of soil (dimensionless); ρ_b is the density of soil matrix (kg m^{-3}); q_s and q_b are the deposition and erosion rates ($\text{kg m}^{-2} \text{s}^{-1}$), respectively.

Mass conservation for sediment yields to

$$\frac{\partial(hS)}{\partial t} = \frac{\partial}{\partial x_i} (u_i h S) - \frac{\partial}{\partial x_i} (h D_i \frac{\partial S}{\partial x_i}) + q_s - q_b$$

where S is the suspended sediment concentration (kg m^{-3}); D_i is the coefficient of horizontal dispersion ($\text{m}^2 \text{s}^{-1}$).

The erosion rate and deposition rate are defined by the following relationships:

for non-cohesive sediments

$$q_s = \max\{0, w_0(S - S^*)\}; \quad q_b = \max\{0, E_r w_0(S^* - S)\}$$

for cohesive sediments

$$q_s = \max\{0, w_0 S - I \frac{\tau}{\tau_d}\}; \quad \text{for deposition (Krone, 1962)}$$

$$q_b = \max\{0, M \frac{\tau}{\tau_e} - I\}; \quad \text{for erosion (Partheniades, 1962)}$$

where S^* is the concentration at equilibrium sediment transport capacity (kg m^{-3}); w_0 is the settling velocity of suspended particles (m s^{-1}); E_r is the overland flow erodibility coefficient; τ_d, τ_e are the critical shear stress for deposition and erosion, respectively; τ is the bed shear stress (N m^{-2}); M is experimentally determined constant.

The total load transport equation developed by Van Rijn (1984a, 1984b) is used to compute the concentration at equilibrium transport capacity for non-cohesive sediments.

Cohesive sediments are different from non-cohesive sediments in two essential ways: aggregation and consolidation. Fine particles of cohesive sediments tend to form large, low density aggregates because of their surface ionic charges. Consequently, the settling velocity of muddy sediments is a function of concentration, salinity, and flow stress. After deposition, cohesive sediments will consolidate, leading to a progressive increase in density and shear resistance with depth and time. Due to our limited understanding of the erosion, deposition, and consolidation processes of cohesive sediments, the modelling of cohesive sediment transport is in its early stage. Recent advances in this field are summarized by Menta and Dyer (1990).

Data in the literature indicate (Menta et al., 1989) that the shear stress for deposition is about $\tau_d = 0.06$ to 0.08 N/m^2 . This correlates well with the experiments of Partheniades, who found that the critical shear stress for deposition is around 0.1 N/m^2 . For mixed sediments with broad size distribution, Menta and Partheniades (quoted in Menta et al., 1989) found that τ_d ranged from about 0.18 to 1.1 N/m^2 .

The critical shear stress for erosion, τ_e , has been related to the specific density of compacted sediments and to the pressure of the overlying water as

$$\tau_e = \tau_D^2$$

If τ_e is in N/m^2 , then the coefficient τ is about 6×10^{-6} to 8×10^{-6} , and the exponent τ is about 2.3 to 2.4 (Menta et al., 1989). τ_D is the dry density of consolidated sediment in kg/m^3 , which is a function of time.

The dry sediment density can be calculated from the bulk density as follows (Menta et al., 1989):

$$\tau_D = \frac{(\tau_B - \tau) \tau_s}{(\tau_s - \tau)}$$

where ρ is the water density; ρ_B is the bulk (wet) density of the sediment; ρ_s is the sediment density.

The critical shear stress for the erosion of consolidated sediments is one to two orders of magnitude greater than that for deposition.

Values for the erosion constant M for cohesive sediments varies from 1.7×10^{-5} to 3×10^{-3} $\text{kg m}^{-2} \text{s}^{-1}$ (Uncles and Stephens, 1989).

However, it should be pointed out that there is no known reliable way to predict the critical shear stresses for deposition and erosion. The values of τ_d and τ_e depend on mineralogy and degree of consolidation. So in situ measurements of τ_d and τ_e are recommended (Amos and others, 1992).

Radionuclide Transport by Overland Flow

The complex process of radionuclide transport in soluble phase and on suspended sediments is affected by many factors such as advection, diffusion and adsorption-desorption processes. The species transport equation is established by writing a mass balance over a stationary control volume through which the fluid is flowing. When diffusion effects are significant, the use of Fick's law results in the appearance of additional terms. The complete radionuclide transport in the aqueous phase and on suspended sediments by overland flow are described by the equations with the sink-source term describing physical-chemical interactions and erosion-deposition exchange processes

$$\frac{\partial(hC)}{\partial t} + \frac{\partial}{\partial x_i}(u_i h C) - \frac{\partial}{\partial x_i} \left(\frac{\partial C}{\partial x_i} \right) h D_i - \frac{\partial C}{\partial x_i} \frac{\partial h}{\partial x_i} = \lambda h C + a_s h S \frac{\partial k_d^s}{\partial x_i} C + C_s \frac{\partial}{\partial x_i} \left(\lambda (1 - Z^*) a_b \frac{\partial k_d^b}{\partial x_i} C - C_b \right) \quad (3)$$

$$\frac{\partial(h S C_s)}{\partial t} + \frac{\partial}{\partial x_i}(u_i h S C_s) - \frac{\partial}{\partial x_i} \left(\frac{\partial S C_s}{\partial x_i} \right) h D_i - \frac{\partial S C_s}{\partial x_i} \frac{\partial h}{\partial x_i} = \lambda S C_s + a_s h S \frac{\partial k_d^s}{\partial x_i} C + C_s \frac{\partial}{\partial x_i} \left(\frac{1}{b} q_b C_b - q_s C_s \right)$$

where C is the volumetric radionuclide activity in aqueous phase (Bq m^{-3}); C_s is the radionuclide activity in exchangeable phase on suspended sediment (Bq kg^{-1}); C_b is the volumetric radionuclide activity in exchangeable phase in upper soil layer (Bq m^{-3}); Z^* is the thickness of active upper soil layer (m); λ is the radionuclide decay constant (s^{-1}); k_d^s and k_d^b are the partition coefficients for "water-suspended sediment" and "water-upper soil layer" systems, respectively; a_s and a_b are the exchange rates for "water-suspended sediment" and "water-upper soil layer" systems (s^{-1}), respectively.

Contamination of Upper Soil Layer.

Contamination of the active upper soil layer is described by the equations

$$\frac{\partial}{\partial t} (Z^* C_b) + a_b Z^* \frac{\partial k_d^b}{\partial x_i} \frac{\partial C}{\partial x_i} - C_b \frac{\partial}{\partial x_i} \left(\lambda (1 - Z^*) C_b - \frac{1}{b} q_b C_b - q_s C_s \right)$$

Numerical Methods

The flow domain is spatially discretized into a computational domain composed of a number of non-overlapping control volumes. Each control volume surrounds a single grid point, which defines the position of intrinsic property variables. Surfaces between nodes are located at the midpoint between two adjacent nodes. Control volumes are defined by their bounding surfaces (see Figure 1). Positive and negative directions along the x -axis are referred to as *east* and *west*, respectively. Similarly, positive and negative directions along the y -axis are

referred to as *north* and *south*, respectively. The *z*-axis is assumed aligned with negative gravitational vector, where positive and negative directions are referred to as *top* and *bottom*, respectively.

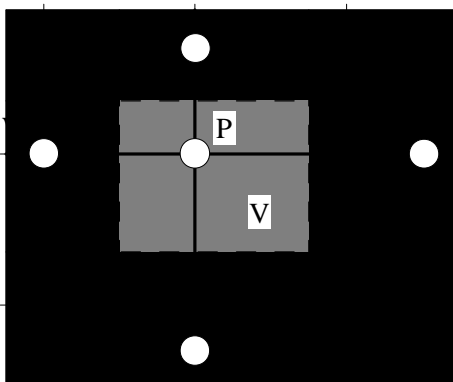


Figure 1. Geometric data for X-Y Cartesian coordinate system.

The shallow water equations (1)-(2) are discretized by implicit finite-difference scheme of the first order of accurate. Due to approximation of advective flux terms by upwind or donor-cell differences, the finite difference scheme is a monotonic scheme. The main advantage of this scheme, as well as widely used in last time TVD-schemes (Harten, 1983,1987; Osher, 1984; Roe,1981; Sweby, 1984; Toro, 1992; Yee, 1989; Zhao, 1996), is its ability to simulate open flow with free boundary. The developed numerical scheme has been used recently to simulate the runoff from small watersheds (Kivva and Zheleznyak, 2002) and relevant radionuclide transport (van der Perk et al., 2000).

The species mass conservation equations are integrated numerically using implicit difference schemes of the first order of accurate. The diffusive flux terms are central differenced, whereas the advective flux terms are upwind or donor-cell differenced. The resulting schemes are also monotonic schemes.

All these schemes are based on the integral form of the conservation equations. By discretization of the integral form of conservation equations, the mass, momentum and species mass remain conserved.

Overland Flow

Rewrite the equations (1)-(2) in the following form

$$\frac{\partial h}{\partial t} + \frac{\partial}{\partial x}(uh) + \frac{\partial}{\partial y}(vh) = 0 \quad (4)$$

$$\frac{\partial}{\partial t}(uh) + \frac{\partial}{\partial x}(uuh) + \frac{\partial}{\partial y}(vuh) + gh \frac{\partial}{\partial x}(h) = f_u \quad (5)$$

$$\frac{\partial}{\partial t}(vh) + \frac{\partial}{\partial x}(uvh) + \frac{\partial}{\partial y}(vvh) + gh \frac{\partial}{\partial y}(h) = f_v \quad (6)$$

Then, the overland flow equations (4)-(6) are discretized by integration them over a control volume *V* and a short time interval Δt .

$$\frac{\partial}{\partial t} \left(\frac{\partial h}{\partial x} \right) + \frac{\partial}{\partial x} (uh) + \frac{\partial}{\partial y} (vh) dV dt$$

$$\frac{\partial}{\partial t} \left(\frac{\partial h}{\partial x} \right) + \frac{\partial}{\partial x} (uh) + \frac{\partial}{\partial y} (vh) dV dt = 0 \quad (7)$$

$$\frac{\partial}{\partial t} \left(\frac{\partial h}{\partial x} \right) + \frac{\partial}{\partial x} (uh) + \frac{\partial}{\partial y} (vh) + gh \frac{\partial}{\partial x} (h) + f_u dV dt = 0 \quad (8)$$

$$\frac{\partial}{\partial t} \left(\frac{\partial h}{\partial x} \right) + \frac{\partial}{\partial x} (uh) + \frac{\partial}{\partial y} (vh) + gh \frac{\partial}{\partial x} (h) + f_u dV dt = 0$$

$$\frac{\partial}{\partial t} \left(\frac{\partial h}{\partial y} \right) + \frac{\partial}{\partial x} (uh) + \frac{\partial}{\partial y} (vh) + gh \frac{\partial}{\partial y} (h) + f_v dV dt = 0 \quad (9)$$

$$\frac{\partial}{\partial t} \left(\frac{\partial h}{\partial y} \right) + \frac{\partial}{\partial x} (uh) + \frac{\partial}{\partial y} (vh) + gh \frac{\partial}{\partial y} (h) + f_v dV dt = 0$$

Using fully implicit temporal discretization and approximating the integrals as summations over the control volume V for nodal point P , the equations (7)-(9) can be rewritten as

$$\begin{aligned} & V \frac{h_P^{t+\Delta t} - h_P^t}{\Delta t} + A_E u_E^2 h_P + u_E^2 h_E^{t+\Delta t} + A_W u_W^2 h_W + u_W^2 h_P^{t+\Delta t} \\ & + A_N v_N^2 h_P + v_N^2 h_N^{t+\Delta t} + A_S v_S^2 h_S + v_S^2 h_P^{t+\Delta t} = 0 \end{aligned} \quad (10)$$

$$\begin{aligned} & V \frac{(uh)_P^{t+\Delta t} - (uh)_P^t}{\Delta t} + A_E (uh)_E^2 u_P + (uh)_E^2 u_E^{t+\Delta t} + A_W (uh)_W^2 u_W + (uh)_W^2 u_P^{t+\Delta t} \\ & + A_N (vh)_N^2 u_P + (vh)_N^2 u_N^{t+\Delta t} + A_S (vh)_S^2 u_S + (vh)_S^2 u_P^{t+\Delta t} \\ & + gh_P^{t+\Delta t} (h)_E^{t+\Delta t} + gh_P^{t+\Delta t} (h)_W^{t+\Delta t} + Vf_{uP}^{t+\Delta t} = 0 \end{aligned} \quad (11)$$

$$\begin{aligned} & V \frac{(vh)_P^{t+\Delta t} - (vh)_P^t}{\Delta t} + A_E (uh)_E^2 v_P + (uh)_E^2 v_E^{t+\Delta t} + A_W (uh)_W^2 v_W + (uh)_W^2 v_P^{t+\Delta t} \\ & + A_N (vh)_N^2 v_P + (vh)_N^2 v_N^{t+\Delta t} + A_S (vh)_S^2 v_S + (vh)_S^2 v_P^{t+\Delta t} \\ & + gh_P^{t+\Delta t} (h)_N^{t+\Delta t} + gh_P^{t+\Delta t} (h)_S^{t+\Delta t} + Vf_{vP}^{t+\Delta t} = 0 \end{aligned} \quad (12)$$

where A_p is the surface between volume elements V_p and V_p ; $U^+ = \max(0, U)$ and $U^- = \min(0, U)$. The advective flux terms in the equations (10)-(12) are upwind or donor-cell differenced.

Taking into account that

$$\frac{(uh)_P^{t+\Delta t} - (uh)_P^t}{\Delta t} \approx h_P^t \frac{u_P^{t+\Delta t} - u_P^t}{\Delta t} \approx u_P^{t+\Delta t} \frac{h_P^{t+\Delta t} - h_P^t}{\Delta t}$$

$$\frac{(vh)_P^{t+\Delta t} - (vh)_P^t}{\Delta t} \approx h_P^t \frac{v_P^{t+\Delta t} - v_P^t}{\Delta t} \approx v_P^{t+\Delta t} \frac{h_P^{t+\Delta t} - h_P^t}{\Delta t}$$

the equations (11)-(12) can be writing in the final form

$$V \frac{u_P^{t+\Delta t} - u_P^t}{\Delta t} \approx \frac{A_E}{h_P^t} \left\{ (uh)_E^- u_P - (uh)_E^+ u_E \right\} \Delta t \approx \frac{A_W}{h_P^t} \left\{ (uh)_W^- u_W - (uh)_W^+ u_P \right\} \Delta t$$

$$\approx \frac{A_N}{h_P^t} \left\{ (vh)_N^- u_P - (vh)_N^+ u_N \right\} \Delta t \approx \frac{A_S}{h_P^t} \left\{ (vh)_S^- u_S - (vh)_S^+ u_P \right\} \Delta t \quad (13)$$

$$\approx g \frac{h_P^{t+\Delta t}}{h_P^t} (h_{E^-})^{t+\Delta t} \approx g \frac{h_P^{t+\Delta t}}{h_P^t} (h_{W^-})^{t+\Delta t} \approx V \frac{u_P^{t+\Delta t} - h_P^{t+\Delta t} u_P^t}{h_P^t} \approx V \frac{f_{uP}^{t+\Delta t}}{h_P^t} \approx 0$$

$$V \frac{v_P^{t+\Delta t} - v_P^t}{\Delta t} \approx \frac{A_E}{h_P^t} \left\{ (uh)_E^- v_P - (uh)_E^+ v_E \right\} \Delta t \approx \frac{A_W}{h_P^t} \left\{ (uh)_W^- v_W - (uh)_W^+ v_P \right\} \Delta t$$

$$\approx \frac{A_N}{h_P^t} \left\{ (vh)_N^- v_P - (vh)_N^+ v_N \right\} \Delta t \approx \frac{A_S}{h_P^t} \left\{ (vh)_S^- v_S - (vh)_S^+ v_P \right\} \Delta t \quad (14)$$

$$\approx g \frac{h_P^{t+\Delta t}}{h_P^t} (h_{N^-})^{t+\Delta t} \approx g \frac{h_P^{t+\Delta t}}{h_P^t} (h_{S^-})^{t+\Delta t} \approx V \frac{v_P^{t+\Delta t} - h_P^{t+\Delta t} v_P^t}{h_P^t} \approx V \frac{f_{vP}^{t+\Delta t}}{h_P^t} \approx 0$$

Advective-Dispersive Transport Equation

Approximation of advective-dispersive transport equation consider on example of discretization of the equation of radionuclide transport in soluble phase .

Integration of the radionuclide transport equation (3) over a control volume V for nodal point P yields

$$\frac{d}{dt} \int_V C \, dV - \sum_i \frac{\partial}{\partial x_i} \left(h D_i \frac{\partial C}{\partial x_i} \right) - \sum_i (u_i C) \frac{\partial C}{\partial x_i} \, dV + \int_V f_C \, dV = 0$$

Using fully implicit temporal discretization, and approximating the integrals as summations over the control volume surface, we obtain the following conservative implicit scheme

$$V \frac{(hC)_P^{t+\Delta t} - (hC)_P^t}{\Delta t} + A_\gamma F_\gamma^{t+\Delta t} - V(\rho C + f_C)_P^{t+\Delta t}, \quad (15)$$

$$\gamma = W, E, S, N$$

where A_γ is the surface between volume elements V_P and V_γ .

The surface flux terms F_γ contain both diffusive and advective flux terms. The diffusive flux terms are central differenced, whereas the advective flux terms are upwind or donor-cell differenced.

$$F_\gamma = \gamma \mathcal{H}_{D_i} \left[\frac{C_P - C_\gamma}{\Delta r_{P\gamma}} + \mathcal{H}_{u_i} \frac{C_\gamma - C_P}{\Delta r_{P\gamma}} \right] C_P, \quad \gamma = W, E, S, N$$

where $U^+ = \max(0, U)$ and $U^- = \min(0, U)$.

The terms delimited with brackets indicate a suitable interface averaging (arithmetic, harmonic, geometric, or upwind). $\Delta r_{P\gamma}$ is the distance between the nodal points P and γ , and $g_{P\gamma}$ is the component of gravitational acceleration in the direction from P to γ .

Due to approximation of advective flux terms by upwind or donor-cell differences, the finite difference scheme (15) is a monotonic scheme of first order accurate in space and time.

Approximation of the Boundary Condition

The discretization of the water flow and species transport equations described above were obtained for nodes positioned within the interior of the computational domain. For nodes located adjacent to the domain boundary, the discretization of the governing equations differs to account for conditions at the boundary. Boundary conditions are specified either with field variables or with surface fluxes on the boundary surfaces. Boundary conditions of the former type are referred to as Dirichlet, whereas the latter type are referred to as Neumann.

Implementation of Dirichlet boundary conditions requires relatively few modifications to the discretized governing conservation equations. These modifications are replacing the following field variables at the boundary nodes by their values on the boundary surfaces.

Neumann-type boundary conditions are accommodated by substituting the specified surface fluxes directly into the discretized form of the conservation equation.

Numerical solution of the discretized equations

The algebraic expressions that result from discretizing the shallow water equations are non-linear. The non-linear algebraic forms of the shallow water equations are converted to a linear form using a multivariable, residual-based, Newton-Raphson iteration technique. The technique will generally yield quadratic convergence of residuals with iteration, given initial estimates of the unknown variables that are sufficiently close to the solution. Each iteration requires the solution of the linearized algebraic form of the shallow water equations.

The finite difference discretization of the overland flow equations leads to a system of non-linear equations:

$$F(x) = 0 \quad F: R^n \rightarrow R^n \quad (16)$$

The non-linear equations (16) are solved iteratively, using a multivariable, residual-based Newton technique

$$x_i^{s+1} - x_i^s \leq p_s \quad s = 0, 1, 2, \dots$$

$$p_s \leq \epsilon \|J(x^s)^{-1} F(x^s)\|$$

where s denotes an iteration number; and $J(x^s)$ is the Jacobian of $F(x)$.

Iteration continues until the criterion is satisfied

$$\max_{1 \leq i \leq n} \frac{|x_i^{s+1} - x_i^s|}{|x_i^s|} \leq \epsilon$$

where ϵ is a user-provided error tolerance.

The iteration routine starts, at a given time step, with an estimate of overland flow depth and flow velocities based on the previous time step. This estimate is used to update values of the governing equation residuals and to evaluate all of the partial derivatives that make up the Jacobian matrix. The resulting system of linear equations is then solved by using the conjugate gradient method with incomplete LU factorization. Solution of the system of equations yields changes to the liquid pressures. An iteration ends by updating the overland flow depth and flow velocities with the changes computed from the system of linear equations. If the criterion is satisfied, then the procedure is determined to have converged and a new time step begins. Otherwise, another iteration commences. If the criterion is not satisfied within a specified number of iterations, the system is considered non-convergent. Non-convergent systems are handled by reducing the simulation step, resetting the liquid pressures to their previous time-step values, and reinitiating the time-step procedures.

The solution to the sediment transport and the shallow water equations are coupled because erosion and sedimentation within flow domain affects the bottom elevation. The flow in turn will alter the sediment transport. Therefore, the numerical solution should reflect this coupling. The developed scheme is a semi-coupled model. The flow equations are modified by updating the bed slope in the momentum equations with the bed elevation computed from the sediment routing equations. The sediment equations, in turn, use the average flow rate and water surface elevations over a given time step to compute the relevant sediment transport information.

References to Annex 1

1. Amos, C.L., Grant, J., Daborn, G.R., and Black, K. (1992) Sea carousel – a benthic, annular flume, *Estuarine, Coastal and Shelf Science*, v.34, no. 6, 557-577.
2. Harten A., High resolution schemes for hyperbolic conservation laws., *Journ. Comp. Physics*, Vol. 49, 1983, 357-393.
3. Harten A., Osher S., Uniformly high-order accurate nonoscillatory schemes., *SIAM Journ. Num. Analysis*, Vol. 24(2), 1987, 279-309.
4. Kivva S.L., Zheleznyak M.J. (2001) Numerical modelling of the 2-D open flow with the moving boundaries: simulation of the watershed runoff and tsunami wave runoff. *Computational Technologies*, Novosibirsk, , v.6., No2, p. 343-350 (In Russian).
5. Krone, R.B. (1962) Flume studies of the transport of sediment in estuarial shoaling processes, Hydraulic Engineering Laboratory and Sanitary Engineering Research Laboratory, University of California at Berkeley, California.
6. Mehta, A.J., and Dyer, K.R. (1990) Cohesive sediment transport in estuarine and coastal waters, in *The sea: John Willey & Sons*, New York, v.9, 815-839.

7. Mehta, A.J., et al. (1989) Cohesive sediment transport. I: Process description, *J. Hydraul. Eng. Div. ASCE* 115(8), 1076-1093.
8. Osher S., Chakravarthy S., High resolution schemes and the entropy condition., *SIAM Journ. Num. Analysis*, Vol. 21(5), 1984, 955-984.
9. Partheniades, E. (1962) A study of erosion and deposition of cohesive soils in salt water, Thesis presented to the University of California at Berkeley, California.
10. Partheniades, E. (1965) Erosion and deposition of cohesive soils, *J. Hydraul. Div. ASCE* 91, 105-139.
11. Partheniades, E. (1971) Unified view of wash load and bed material load, *J. Hydraul. Div. ASCE* 103(HY9), 1037-1057.
12. Roe P.L., Approximate Riemann solvers, parameter vectors, and difference schemes., *J. Computational Physics*, Vol. 43, 1981, 357-372. 205
13. Sweby P.K., "High resolution schemes using flux limiters for hyperbolic conservation laws.", *SIAM Journ. Num. Analysis*, Vol. 21(5), 1984, 995-1011.
14. Toro E., Riemann problems and the WAF method for solving the two-dimensional shallow water equations., *Philosophical Trans. Royal Soc., London, U.K.*, A338, 1992, 43-68.
15. Uncles R.J., J.A.Stephens (1989) Distribution of suspended sediment at high water in a macrotidal estuary, *J. Geophys. Res.*, 94(C10), 14395-14405.
16. Van der Perk M., Jetten V., Karsenberg D., Walling E., Laptev G., Voitsekhovich O., Svetlichnyi A., Slavik O., Linnik V., Korobova E., Kivva S., Zheleznyak M. (2000) Assessment of spatial redistribution of Chernobyl –derived radiocaesium within catchments using GIS-embedded models. – *The Role of Erosion and Sediment Transport in Nutrient and Contaminant Transfer.*, IAHS Publ.No.263, pp.277-284.
17. Van Rijn, L.C. (1984a) Sediment Transport, Part I: Bed Load Transport. *J. Hydr. Engrg.*, ASCE, 110(10), 1431-1456.
18. Van Rijn, L.C. (1984b) Sediment Transport, Part II: Suspended Load Transport. *J. Hydr. Engrg.*, ASCE, 110(11), 1613-1641.
19. Yee H.C., "Semi-implicit and fully implicit shock-capturing methods for nonequilibrium flows.", *AIAA Journal*, Vol. 27(3), 1989, 299-307.
20. Zhao D.H., Shen H.W., Tabios G.Q., Lai J.S., Approximate Riemann solvers in FVM for 2D hydraulic shock wave modelling., *J. Hydr.Eng.* Vol. 122(12), 1996, 692-702.
21. Zheleznyak M. (1997) Multiple scale analyses of radioactive contamination for rivers and reservoirs after the Chernobyl accident. - Multiple Scale Analyses and Coupled Physical Systems. Proc. Saint-Venant Symposium, August 28-29, 1997, Presses de l'école nationale des ponts et chaussees, Paris, 1997, p.p. 45-52.
22. Zheleznyak M. et al. (1992) Mathematical modeling of radionuclide dispersion in the Pripyat-Dnieper aquatic system after the Chernobyl accident. -*The Science of the Total Environment*, v.112, p.89-114.
23. Zheleznyak M., Heling R., Raskob W. (2002) Hydrological Dispersion Module of the Decision Support System RODOS- Proc. Conf. ECORAD-2001, Aix-de Provance, France, 3-6 September, 2001 (In Press)
24. Zheleznyak M., Shepeleva T., Sizonenko V., Mezhueva I. (1997) Simulation of countermeasures to diminish radionuclide fluxes from Chernobyl zone via aquatic pathways - *Radiation Protection Dosimetry*, 1997, v.73, No.1-4, pp.181-186

